Environmental Science and Pollution Research (2023) 30:22458–22470
https://doi.org/10.1007/s11356-022-23747-6

RESEARCH ARTICLE

Study on microstructure and extinction characteristics of particulate matter in diesel engine fueled with different biodiesels

Siqi Ye[1] · Dengpan Zhang[1] · Bo Chen[1] · Jieping Xu[1] · Changkai Jia[1,2] · Deqing Mei[1] · Yinnan Yuan[1,3]

Received: 5 July 2022 / Accepted: 17 October 2022 / Published online: 27 October 2022

Abstract

Biodiesel combustion particulate matter (PM) is different from diesel combustion PM in terms of microscopic morphology, which directly affects the optical properties of PM. To investigate the effect of the microstructure of biodiesel PM on the extinction characteristics, an experiment was performed on a high-pressure common rail diesel engine to collect PM from three kinds of biodiesel (the main raw materials were soybean oil methyl eater (SME), palm oil methyl eater (PME), and waste cooking oil methyl eater (WME), respectively). The particle size distribution, micro morphology, and extinction characteristics of biodiesel PM were analyzed. Results show that combustion biodiesel reduces PM emissions by up to 84.2%. Compared to PM from diesel, biodiesel PM has a smaller particle size and a higher aggregation degree, which results in weaker light absorption capacity. With the iodine number of biodiesel decreasing, the number concentration of biodiesel PM decreases and the fractal dimension increases, which leads to producing a more complex agglomerate and a consequent reduction in extinction coefficient. The average particle sizes of PM from SME, PME, and WME are 5.1%, 6.7%, and 13.9% lower than that of diesel PM. Compared with diesel combustion PM, the peak absorption coefficients of SME, WME, and PME combustion PM decrease by 8.4%, 11.4%, and 13.3%, respectively. The extinction properties of particles decrease with increasing fractal dimension within the wavelength range of visible light.

Keywords Biodiesel · Iodine number · Particulate matter · Microstructure · Extinction coefficient

Introduction

Particulate matter (PM) emissions from diesel engines are classified as a group of carcinogens (Scheepers and Vermeulen 2012). Chronic exposure to PM2.5 may lead to respiratory, cardiovascular, and neurological diseases (Miyashita et al. 2021), as well as an increased incidence of novel coronavirus pneumonia (COVID-19) (Stieb et al. 2020; Cristina et al. 2021). Moreover, the greenhouse effect of PM emissions from engines leads to global warming, which is second only to carbon dioxide, and it is urgent to reduce PM emissions of engines.

Combustion oxygenated fuels are one of the pretreatment technologies to control diesel PM emissions (Tan et al. 2014; Huang et al 2016). Biodiesel is a typical green oxygenated fuel (Zhang et al. 2018) with the advantages of renewable (Moore et al. 2017), low air pollutant emission (Nabi et al. 2017), good lubrication, and complete biodegradation (Srinivasan et al. 2021). Biodiesel can be produced from a wide variety of feedstock sources, such as vegetable oils, animal fats, and industrial waste oils (Alptekin et al. 2012; Moser 2014). The physical and chemical properties of biodiesel are similar to diesel fuel, so that diesel engines can directly use biodiesel without engine modification. Diesel engines fueled with biodiesel or biodiesel/diesel blends can significantly reduce HC, CO, and PM emissions (Alptekin 2017). Engines are dependent on a shift in the fuel sector to achieve "emission peak and carbon neutrality" (Nutakki et al. 2021). Application of biodiesel on internal combustion engine has a broad application prospect for alleviating environmental

Responsible Editor: Philippe Garrigues

✉ Dengpan Zhang
zhdp@ujs.edu.cn

[1] School of Automobile and Traffic Engineering, Jiangsu University, Zhenjiang 212013, People's Republic of China

[2] CIMC Offshore Engineering Institute Co., Ltd, Yantai 264000, People's Republic of China

[3] College of Energy, Soochow University, Suzhou 215006, People's Republic of China

pollution and promoting upstream energy change (Chai et al. 2020; He et al. 2017).

With the increasingly stringent engine emission regulations, the requirements for testing for PM size and concentration are becoming higher. The common means of detecting PM are the membrane weighing method and the light monitoring method. The membrane weighing method (Takahashi et al. 2008) uses a precision scale to weigh the difference in mass of the membrane before and after adsorption of the PM to calculate the mass concentration of the PM. The light monitoring method measures the particle size based on the amount of scattered and absorbed light by individual particles to find the size and number of particles in the gas sampling volume and then calculates the concentration of the particles (László et al. 2022). Compared to the membrane weighing method, the light monitoring method is easy to operate, simple in structure, and rapid in measurement. Therefore, the light monitoring method is widely used. Changes in the optical properties of PM affect the accuracy of measurements by their detection and monitoring instruments. Instruments such as smoke meters, particle size spectrometers, and absorption photometers produce data on the smoke value and particle size distribution of PM based on the absorption, scattering, and refraction of light. In contrast, the ability of particles to absorb, scatter, and refract light can be collectively referred to as the extinction properties of PM. The overall morphology of biodiesel PM is similar to that of diesel PM, but there are differences in the major particle sizes and fractal dimensions (Aizawa et al. 2012), both of which are important factors affecting the accuracy for optical detection of PM.

To investigate the effect of particle micro formation on extinction performance, Laborde et al. (2013) applied a single-particle soot photometer (SP2) and differential migration analyzer (DMA), and they found differences in particle size and morphology of PM altered the effect of light absorption by the PM. Wang et al. (2021) used an SP2 and a centrifugal particle mass analyzer (CPMA) and concluded that the light absorption effect of single particles increases with larger incident light wavelength. Kuang et al. (2020) used X-ray photoelectron spectroscopy and UV–Vis spectrometer to study the absorption effect of incident light by PM emitted from the combustion of different fuels. PM emitted from a mixture of biodiesel and diesel fuel was found to possess a higher extinction capacity compared to that of diesel fuel. Therefore, the differences in microstructure of biodiesel PM can lead to significant differences in the extinction effect compared to that of ordinary diesel PM.

To further investigate the optical properties of complex-shaped particles at the nanoscale, the finite difference time domain (FDTD) method has been widely used for optical property calculations. Fredriksson et al. (2009) performed simulations by using the FDTD method, and the results showed that the spectral absorption peaks of graphite nanostructures appeared to a red-shift with increasing particle size, and the intensity of the absorption peaks increased with increasing particle size. Qiu et al. (2010) found that the FDTD method could obtain the light scattering data of the nanoscale structure, which was perfectly matched with the numerical results calculated by using rigorous coupled wave analysis (RCWA). Therefore, the FDTD Solution software has the advantages of convenience and reliability and is suitable for the optical simulation of nanoscale particles.

In conclusion, the microscopic characteristics of particles affect the particle optical properties that directly determine the objectivity of particle detection method based on extinction principle. When the optical detection method being suitable to diesel PM is used to detect biodiesel PM, there will be a much difference between the detecting emissions and the true emissions, which does not objectively present the real situation of biodiesel PM emissions. However, the research on the optical properties of biodiesel combustion particles needs to be deepened; especially the extinction characteristics of different kinds of biodiesel combustion particles are rarely reported. The aim of this study was to analyze the influence of microstructure of biodiesel combustion particles on extinction characteristics. Three kinds of biodiesel made from typical material were taken as test fuel, and then an engine bench test was carried out and collected PM. The particle size distribution, micro morphology, and extinction characteristics of three kinds of biodiesel exhaust PM were analyzed in order to provide a basis for objective evaluation of biodiesel PM emissions from engines.

Methods

Experimental setup

PM was collected on an electronically controlled common-rail diesel engine by burning different test fuels. The cetane number, kinematic viscosity, and low calorific value of biodiesel decrease with increasing unsaturation, while the density and bulk modulus increase (Wu et al. 2019). The iodine number can be used as a reference quantity to measure the physicochemical properties of biodiesel. The iodine number is the mass of iodine in grams required to completely saturate 100 g of biodiesel by a stoichiometric reaction (Gopinath et al. 2015). The cetane number, oxygen content, and low heating value of biodiesel are related to the number of C = C double bonds and can be obtained by calculation. The physicochemical properties of the fuel such as component, iodine number, density, and kinematic viscosity were measured at 293 K using gas chromatography-mass spectrometry, Wechsler iodine measurement, MDJ-300G liquid

Table 1 Fuel properties

Item	SME	PME	WME	Diesel
Cetane number	53.20	54.64	57.55	51
Oxygen content (%)	10.96	10.98	11.08	0
Lower heating value (MJ/kg)	37.45	37.25	37.17	43.5
Density (kg/m^3)(20°C)	875	877	873	845
Kinematic viscosity (mm^2/ s)	5.9	5.83	5.80	3.51
Iodine number (g/100 g)	100.9	95.3	80.8	/

densitometer, and NDJ-5S rotational viscometer, etc. The results are shown in Table 1.

Figure 1 shows the bench test system, and the main technical parameters of the test engine are shown in Table 2. The engine speed was controlled at 2400 r·min^{-1}, and the engine torque was selected at 250 N m to collect sufficient particles. At this operating point, the particle size data were measured online by an EEPS 3090 particle size spectrometer. The sampling device was placed upstream of the exhaust aftertreatment unit and allowed direct sampling of PM in the engine exhaust, and the probe sampling device is shown in Fig. 2. The thermophoresis sampling device cooled the sampling tube by cooling water, and when the high-temperature exhaust of the engine flowed through the sampling tube, the PM in the exhaust adhered to the inner wall of the sampling tube under the action of thermophoresis force. After 1.5 h of stable engine operation, the PM on the wall of the sampling tube was collected for off-line analysis. The probe sampling

Table 2 Main technical parameters of the test diesel engine

Item	Specification
Model	Inline, water-cooled, turbocharged
Injection system	Common-rail direct injection
Number of cylinder	4
Bore × stroke (mm × mm)	95 × 100
Displacement (L)	2.83
Compression ratio	17.5: 1
Max. torque/speed (N m/r·min^{-1})	≥ 250/1600–2400
Max. power (kW/r·min^{-1})	75/3200

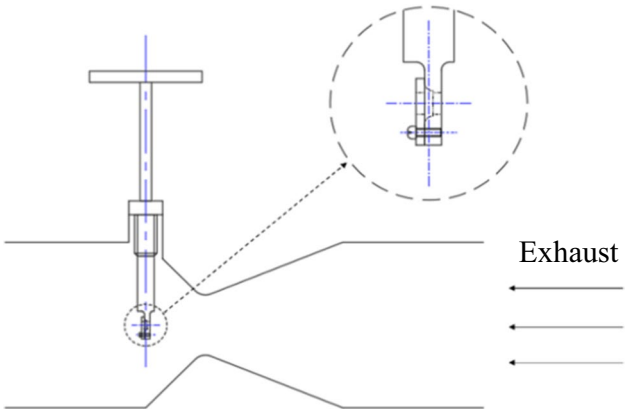

Fig. 2 Schematic of the probe sampling device

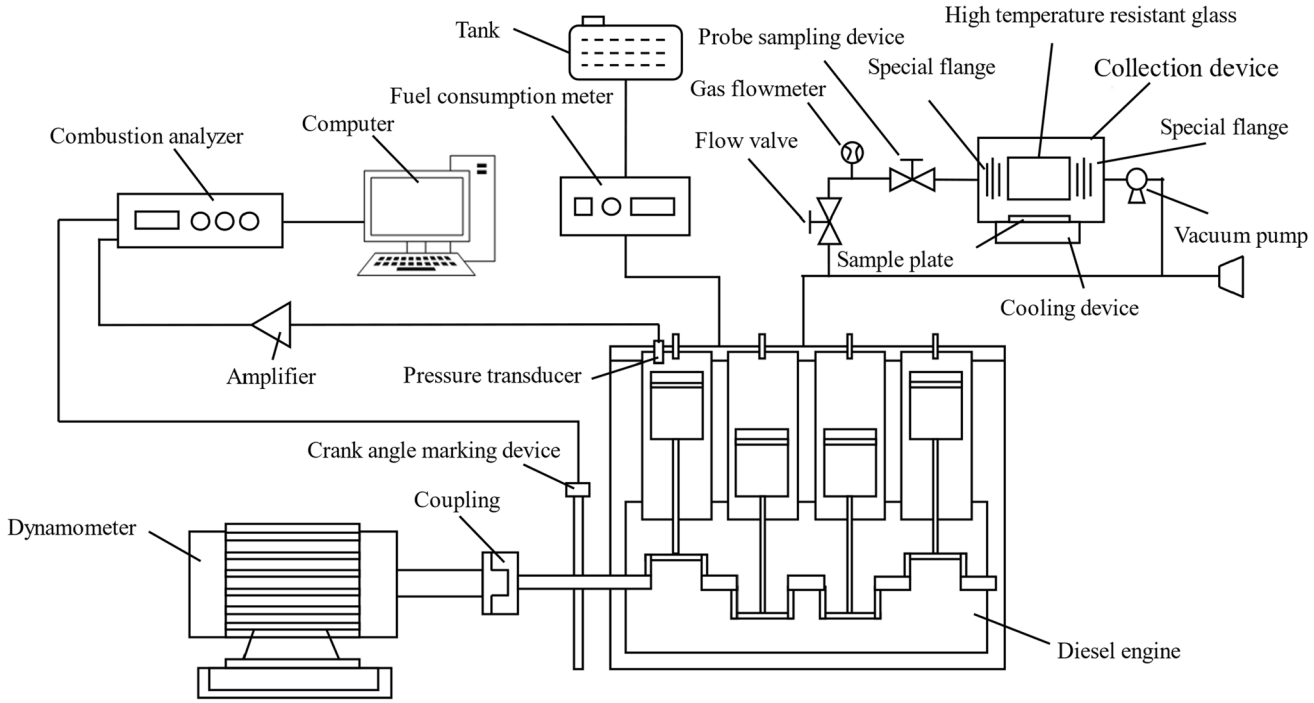

Fig. 1 Schematic diagram of the bench test system

device is inserted directly into the exhaust pipe to take samples while the engine is running, and the PM adheres to the copper mesh at the lowermost end of the sampling device by the airflow. After several pre-experimental tests, the sampling time was determined to be 10 s per sample. When the different oil samples were changed, the sampling tube of the particulate collection device was cleaned, and the engine was run on the test oil for 20 min before starting to collect the particulate samples.

The collected PM by the probe sampling device was applied to a high-resolution transmission electron microscope (JEM-2100(HR)) to obtain TEM images, which were then processed by Digital Micrograph software and MATLAB program to obtain the microstructural information of the PM. The particles collected by the thermophoretic sampling device were measured with a UV–Vis spectrometer, which measured information on the light absorption and reflection of PM from different fuels.

Analysis method and procedure

From electromagnetic theory, it is known that the refractive index is one of the most important physical parameters that determine the ability of a granule to scatter or absorb light (Zhang et al. 2021). The refractive index consists of two main components: the real part, which represents the ability of the particle to scatter light, and the imaginary part, which represents the ability of the particle to absorb light, denoted as $m = n - ki$ (Zhang et al. 2021). The real and imaginary parts of the refractive index do not exist independently of each other, and they satisfy the Kramers–Kronig relationship (K-K relationship for short) (Anis et al. 2021). The absorption spectrum of the PM is first measured by applying a spectrophotometer test, and then the scattering spectrum of the PM is derived by inversion of the K-K relationship, and finally, the refractive index of the PM is obtained. Figure 3 shows the UV–Vis absorption spectra of the diesel sample (DS), soybean oil methyl ester sample (SMES), palm oil methyl eater sample (PMES), and waste cooking oil methyl eater sample (WMES), and a group of carbon black (CB) particles was added to the experiment as a reference for comparative analysis.

After obtaining the absorption spectra of PM from four kinds of fuels, the scattering spectra of the PM were derived by applying the inversion of the transmission method based on the K-K relationship (Xing et al. 2010). In the transmission method, according to the Lambert–Beer law, when the incident light of wavelength λ and intensity I_0 passes through particulate suspension with width L, the light intensity I of the transmitted light passing through the sample will decay under the effect of light absorption and scattering by the PM, as shown in Fig. 4.

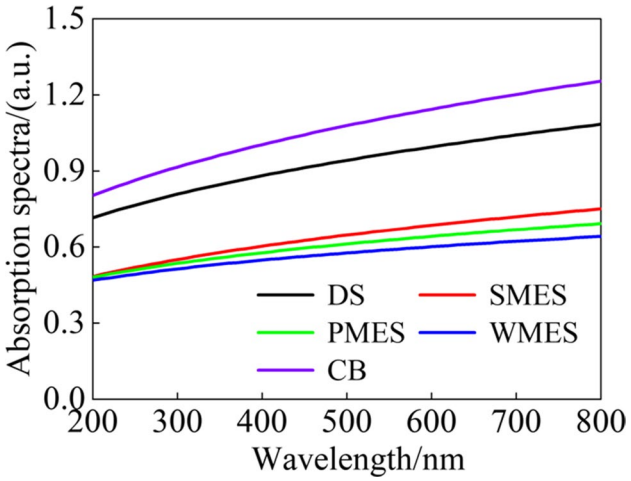

Fig. 3 Absorption spectrum of the refractive index of PM from different fuels

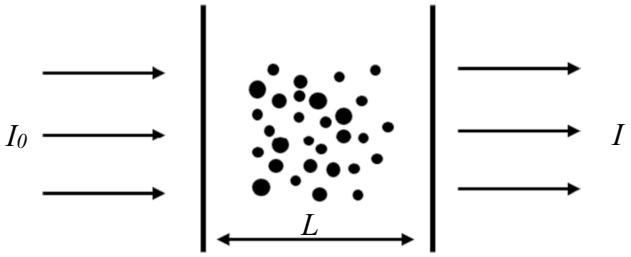

Fig. 4 Schematic diagram of transmission method

The variation of the transmitted light intensity can be expressed as

$$\ln\frac{I(\lambda)}{I_0(\lambda)} = -\tau(\lambda)L \tag{1}$$

In Eq. (1), τ is the turbidity of the medium, which is the total extinction cross-section of all particles per unit volume; $I(\lambda)/I_0(\lambda)$ is the transmission ratio of λ wavelength.

The transmittance ratio of a non-homogeneous particulate sample can be expressed as

$$\frac{I(\lambda)}{I_0(\lambda)} = \exp[-\mathrm{LN}_V \int_{D_{\min}}^{D_{\max}} \frac{\pi}{4} D^2 P(D) Q_{\mathrm{ext}}(\lambda, m, \alpha) dD] \tag{2}$$

In Eq. (2), $\alpha = \pi D/\lambda$ is the particle scale parameter; Q_{ext} is the extinction coefficient, which characterizes the sum of scattering and absorption of incident light by a single particle and is a function of the particle scale parameter α, wavelength λ, and relative medium complex refractive index $m[n(\lambda),k(\lambda)]$, which can be calculated by Mie scattering theory; N_V is the particle number concentration; $P(D)$ is the geometric particle size distribution function of the particle.

The K-K relationship establishes a theoretical connection between the real part n and the imaginary part k of the refractive index. K-K relationship is derived from complex function theory based on dispersion theory, which is based on the physical premise that the effect of an object on incident light is linear and causal (there will be no reflected light waves unless light waves are shining on the object). Taking n and k as variables, the K-K relationship is expressed as

$$n(\lambda) = 1 + \frac{2\lambda^2}{\pi} P \int_{\lambda_l}^{\lambda_h} \frac{\lambda k(\lambda)}{\lambda^2 - \lambda_0^2} d\lambda \tag{3}$$

In Eq. (3), P is the value of the Cauchy master integral; λ_0 is the wavelength of the term before the iteration.

The measured $k(\lambda)$ was brought into Eq. (3) to find the corresponding $n(\lambda)$ by applying Simpson's product method, and then the scattering spectra of PM from different fuels. Refractive indices were plotted, as shown in Fig. 5.

After obtaining the refractive index of the particles, the software of finite difference time domain (FDTD) is applied to calculate the extinction characteristics of the particles. In the modeling process, an insulating boundary layer, a scattering sensing layer, an absorbing sensing layer, a light source, and a time monitor are established, as shown in Fig. 6. Among them, the perfectly matched layer boundary condition (PML) is used for the insulating boundary layer (Chen et al. 2022). In addition, the incident light source uses an unpolarized full-field scattering field light source with a spectral range of 200–800 nm, the polarization direction of the light source is parallel to the x-axis direction, and the incident direction of the light source is downward along the z-axis. Full court area.

To select a suitable grid, the simulated field of PM with a particle size of 100 nm was used as the analysis object, and the mesh grid accuracy was set to 0.4 nm, 0.6 nm, 0.8 nm, and 1.0 nm to calculate the variation curves of extinction coefficient with incident wavelength for the spherical PM model with different size of grid division, and the results are shown in Fig. 7. It can be seen that the accuracy of the particle simulation results in the software is not affected when the grid division accuracy is in the range of 0.4–1.0 nm. Considering the grid accuracy, computer performance, memory, and running time, the grid is set to auto non-uniform grid with a grid accuracy of 3, and a mesh grid with 0.5 nm accuracy ($dx = dy = dz = 0.5$ nm) is added around the particles to improve the reliability and accuracy of the simulation results.

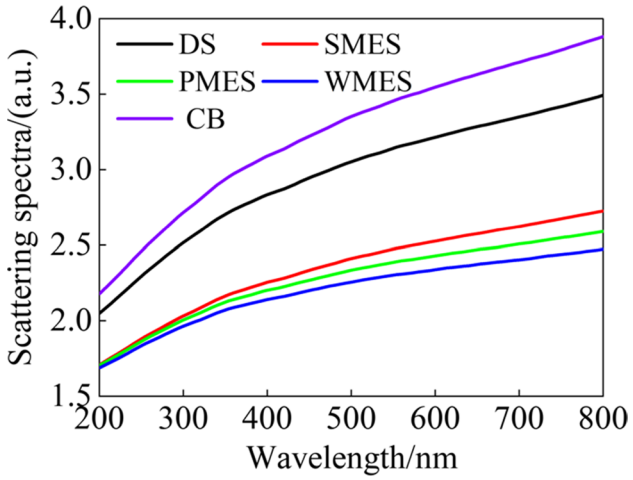

Fig. 5 Scattered spectrum of the refractive index of PM from different fuels

Results and discussion

Particle size distribution analysis

Figure 8 shows the distribution of particle quantity concentration and mass concentration of different fuel emissions measured by EEPS particle size spectrometer. Fifty nanometers can be used to distinguish between particles in the nucleation ($Dp \leq 50$ nm) or accumulation mode

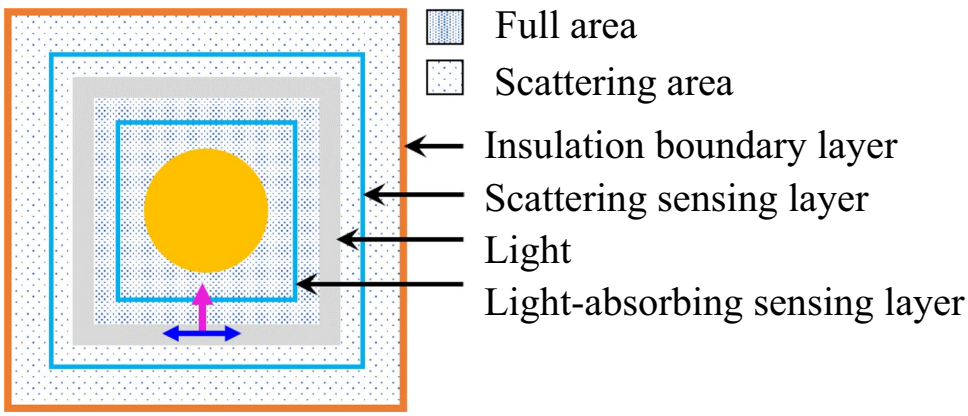

Fig. 6 Sketch of model boundary settings

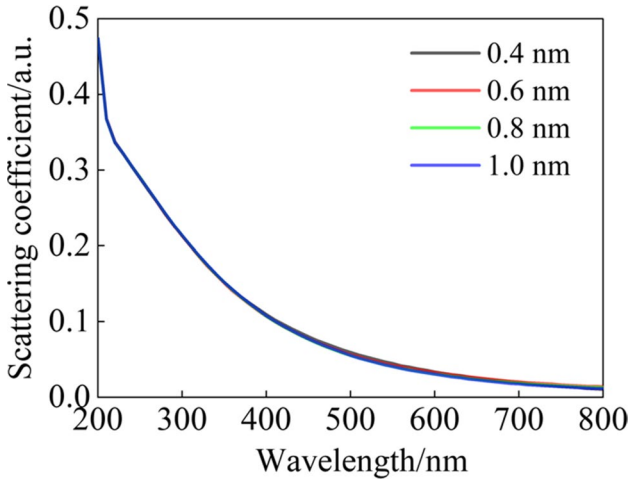

Fig. 7 Effect of different mesh sizes on extinction effect

($Dp > 50$ nm). It can be seen that most of the geometric particle sizes were concentrated in the accumulation mode, and the particle size distribution was isomorphic. The particle size data were processed according to statistical principles to obtain a graph of the variation in the number concentration, mass concentration, and geometric mean particle size of PM emitted from different fuels, the results of which are shown in Fig. 9. The geometric mean particle size of the PM was 59.8 nm, 58.8 nm, 54.3 nm, and 63.0 nm for SME, PME, WME, and diesel, respectively. The PM from biodiesel was less in number concentration, particle size, and mass concentration. This is since biodiesel burnt more adequately during the particulate generation process, which inhibited the growth and consolidation of PM, resulting in lower PM emissions (Mei et al.2006). Nucleated PM with a small particle size was extremely volatile, and biodiesel particle size was influenced by the iodine number, so the biodiesel PM number concentration also decreased with the decrease of iodine number (Du et al. 2021). Combined with Figs. 10 and 11, it can be seen that the amount and average particle size of biodiesel PM increased with increasing iodine number.

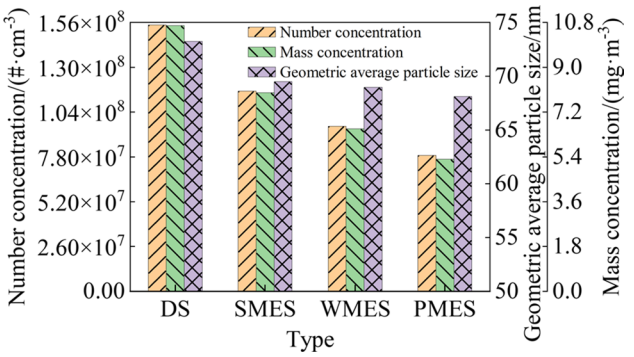

Fig. 9 Number concentration, mass concentration, and geometric average particle size of PM from different fuels

Particle fractal dimension analysis

Figure 10 shows the TEM images of PM from different fuels were obtained by the program processing of the bounded image, and then the fractal dimension of the corresponding PM was calculated. The fitting equations and fitting results are shown in Table 3. The fitting coefficients were all greater than 0.99, which implied the fitting effect was good. As can be seen in Fig. 10, most of the diesel PM showed an identifiable chain-like structure with little to no por. However, the chain-like structure of biodiesel PM aggregated together to form denser agglomerated particles, mainly grape-like and agglomerated structures, while the number of pores between the agglomerates was higher than that of diesel. From the fractal dimension of PM from different fuels in Table 3, we can see that the fractal dimension of biodiesel PM was higher than that of ordinary diesel PM, with a higher degree of agglomeration and more complex shape. This is due to the higher oxygen content of biodiesel compared to diesel, which caused more complete combustion in the cylinder. This resulted in the particle size of the PM becoming smaller, while the specific surface area of the basic particles and contact area between adjacent basic carbon particles increased. The electrostatic and van der Waals force interactions between the

Fig. 8 Distribution diagram of number concentration and mass concentration of different PM

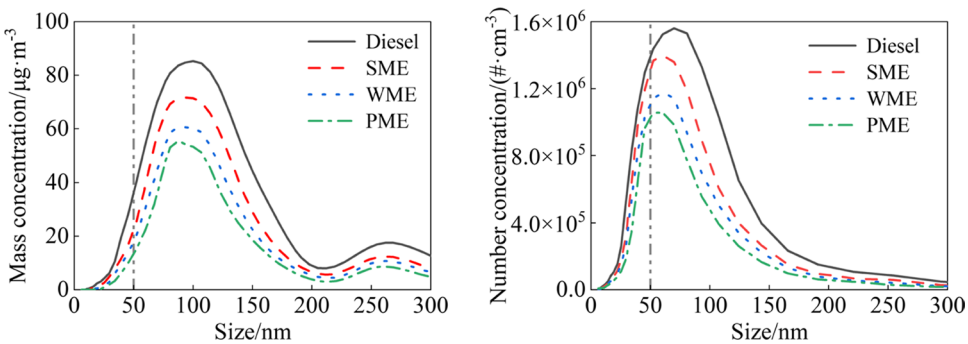

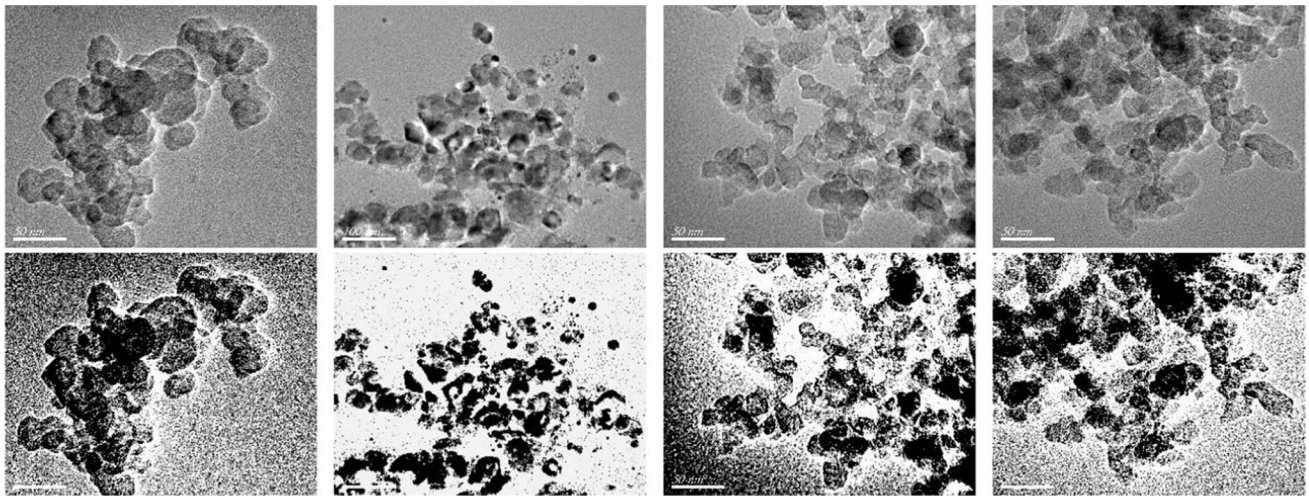

Fig. 10 TEM images of PM from different fuels

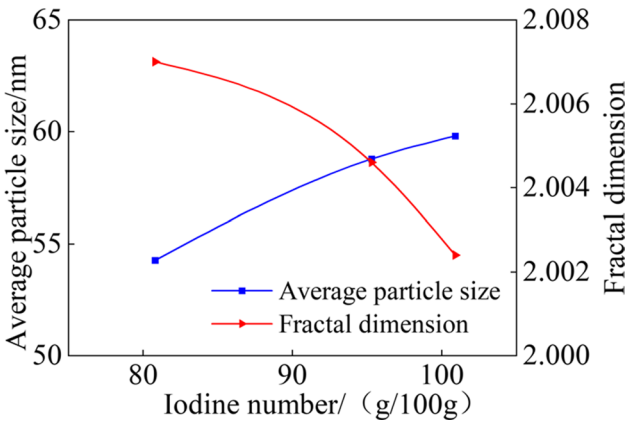

Fig. 11 The relationship between average particle size, fractal dimension, and iodine number

Table 3 Fractal dimensions of different PM

Types	Fitted equation	Fractal dimension	Regression coefficient/R^2
DS	$y=-1.9860x+13.9072$	1.9860	0.9981
SME	$y=-2.0024x+13.9502$	2.0024	0.9989
PME	$y=-2.0066x+13.9552$	2.0046	0.9991
WME	$y=-2.0070x+13.9661$	2.0070	0.9991

elementary carbon particles increased with increasing contact area, resulting in dense agglomerated particles on a macroscopic scale. This is consistent with the research of Mei et al. (2019). In addition, as the oxygen content of biodiesel PM was influenced by the iodine number, the difference in fractal dimension is shown in Fig. 11, and it can be found that the larger the iodine number of biodiesel, the smaller the corresponding fractal dimension, which means the smaller the degree of agglomeration of PM. As a result, diesel PM differs significantly from biodiesel PM in terms of fractal dimension, and these differences can cause changes in extinction properties.

Particle extinction characteristics

Effect of particle size distribution on extinction characteristics

To analyze the effect of different particle sizes on the extinction characteristics of PM, the refractive index of carbon black was used as input data for the PM, and nine PM models in the range of 20–100 nm were built in turn, and the results are shown in Fig. 12. It can be seen from the figure that the scattering coefficient of the particles decreased as the wavelength of incident light increased. The scattering coefficient of PM decreased more rapidly as the particle size increased. In addition, the absorption coefficient of the incident light first rose and then fell with an increasing wavelength of the incident light, and the peak absorption coefficient appeared red-shifted with the increase of the particle size (redshift, the spectrum shifts to the end of the larger wavelength of the light wave, which shows the phenomenon of shifting toward the red light) (Huang and Wang 2021; Lawrence et al.2021). This is because the more significant the particle size, the larger the relative surface area, which results in a greater scattering effect on light. The

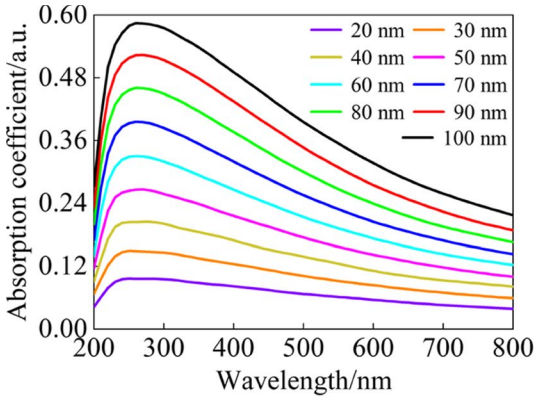

(a) Absorption coefficients for different particle sizes

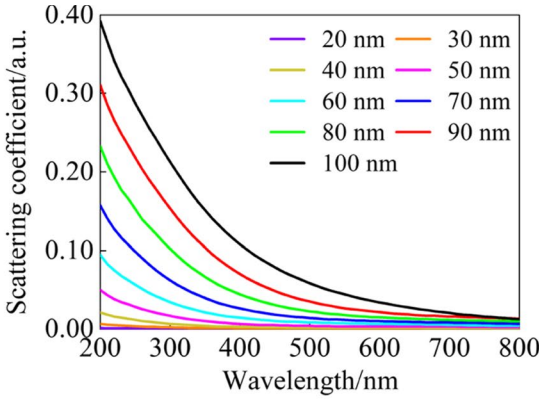

(b) Scattering coefficients for different particle sizes

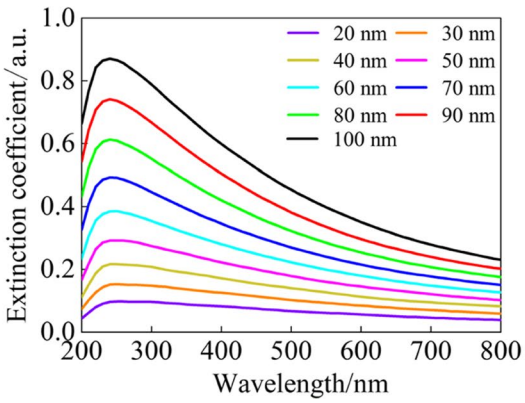

(c) Extinction coefficients for different particle sizes

Fig. 12 Effect of particle size on extinction characteristics

peak absorption occurred in the low wavelength band of incident light because the brown carbon of diesel PM and the aromatic hydrocarbon component of biodiesel PM had a better absorption effect on the low band of incident light. The absorption and scattering coefficients were highly sensitive to variation in particle size, while the change of particle size has little effect on the wavelength position of the absorption peak. The proportion of absorption coefficient in extinction decreased with increasing particle size, implying that absorption played a major role in small particle size, but scattering would gradually become dominant in extinction with increasing particle size. Therefore, the extinction coefficient of PM increases with the particle size, and the particle size of diesel and biodiesel is different, which also leads to the difference in their extinction coefficients. In the visible range (wavelengths is 390–780 nm), the extinction coefficient of particles is positively correlated with particle size, which greatly affects the accuracy of the optical detection instrument. In addition, the particle size distribution is mainly studied for single PM, which is often aggregated into clusters in the exhaust pipe, so we need to investigate the fractal dimension of the particulate agglomerates.

Effect of fractal dimension on extinction characteristics

Influenced by the particle size distribution, the fractal dimension of the particle agglomerates also affects the extinction characteristics. Six TEM images of the particle agglomerates from four fuels with close geometric particle size and clear basic carbon particles were selected, as shown in Fig. 13. The corresponding particulate models were constructed in FDTD Solutions software, and the refractive index of carbon black was used as the input refractive index. The fractal dimensions of the six TEMs

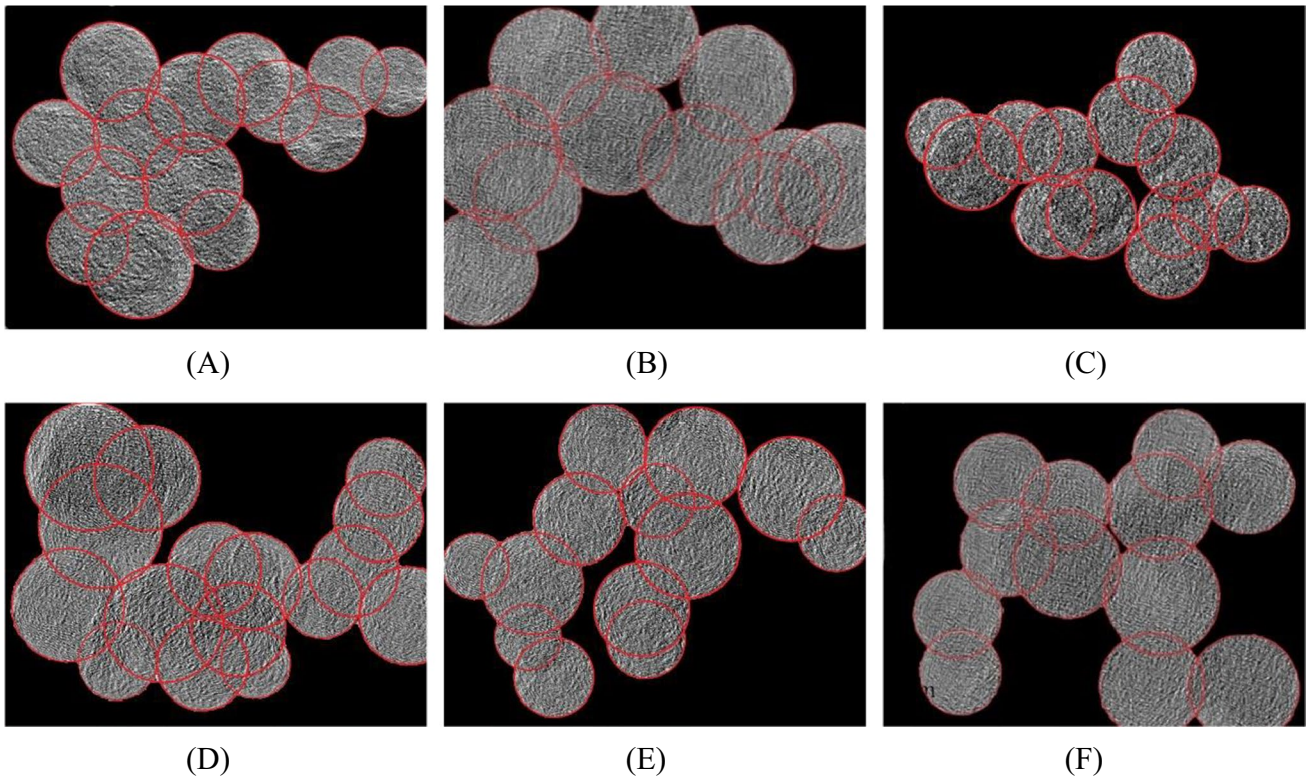

Fig. 13 Images and Models of PM in FDTD software

Table 4 Fractal dimension of different PM

Type	D_B	R^2
A	1.4243	0.9921
B	1.4266	0.9937
C	1.4291	0.9915
D	1.4348	0.9928
E	1.4423	0.9936
F	1.4552	0.9917

were calculated by using MATLAB software and named A, B, C, D, E, and F in descending order of their fractal dimension, as shown in Table 4. The scattering coefficients, absorption coefficients, and extinction coefficients of the PM in different fractal dimensions were obtained after simulation, as shown in Fig. 14. It can be seen from the figure that the scattering coefficient of the particles decreased as the wavelength of the incident light increased. The scattering coefficient of PM decreased at different rates for different fractal dimensions; the larger the fractal dimension of PM, the slower the decreasing speed of the scattering coefficient. The absorption coefficient of the incident light increased and then decreased with an increasing wavelength of the incident light, while the peak absorption coefficient showed a slight red-shift with increasing fractal dimension. This is because a larger fractal dimension means that the basic carbon particles are more aggregated. The contact area of PM with the incident light was reduced, resulting in a consequent reduction in the extinction characteristics. On the other hand, as the fractal dimension increased, the surface of PM became more complex, and the absorption effect of light increased relatively, implying a dominant role of light absorption in extinction characteristics. The fractal dimension of the particles is negatively correlated with the extinction properties. Combined with the previous section, it can be seen that the fractal dimension of biodiesel particles is larger than that of diesel particles, and the aggregation degree is larger and more complex, so the extinction effect on incident light is weaker; among the three kinds of biodiesel PM, as the iodine number of biodiesel decreases, the extinction effect is weaker. In the visible range (wavelengths is 390–780 nm), the extinction properties of particles decrease with increasing fractal dimension, which affects the accuracy of the optical detection instrument.

Extinction characteristics analysis

The difference in size distribution and morphological structure between biodiesel PM and diesel PM inevitably

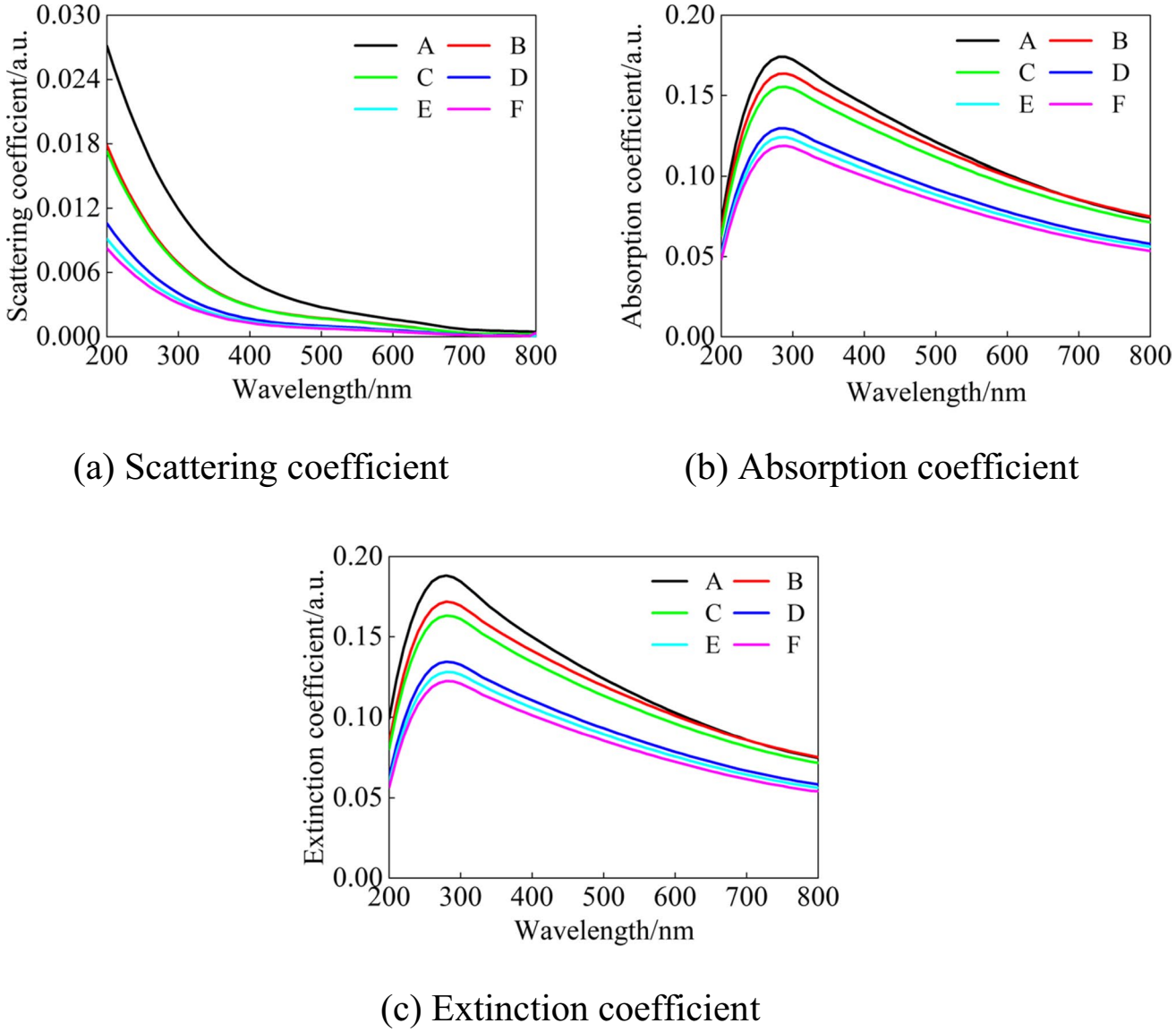

Fig. 14 The difference in extinction effect of PM with different morphologies

leads to the difference in the extinction characteristics. The refractive indices of PM emissions of diesel, SME, WME, and PME were introduced into the model with the 100-nm PM model, and the curves of the variation of the optical properties of PM from different fuels with the incident light were calculated, as shown in Fig. 15. It can be seen that the extinction effect of all three biodiesel PM is lower than that of diesel PM. The peak absorption coefficients of SMES, PMES, and WMES were 1.52, 1.47, and 1.44, respectively, and the wavelengths were 253 nm, 241 nm, and 236 nm; the peak values were lower than those of diesel PM by 8.4% and 11.4%, respectively. The peak absorption coefficients were 8.4%, 11.4%, and 13.3%, respectively, compared with those of diesel PM. The peak wavelengths of the absorption coefficients of the three biodiesel granules for incident light appear to be blue-shifted as the iodine number of the biodiesel decreases. As absorption played a dominant role in the extinction characteristics, the extinction coefficients of the PM also appeared to blue-shift with the decrease in biodiesel iodine number. The extinction effect of biodiesel PM on incident light was weaker than that of diesel PM; among the three kinds of biodiesel, with the decrease of biodiesel iodine number, the scattering coefficient and absorption coefficient of biodiesel PM gradually decreased, and the extinction effect diminished. In the visible light range (wavelength is 390–780 nm), the extinction ability of diesel is higher

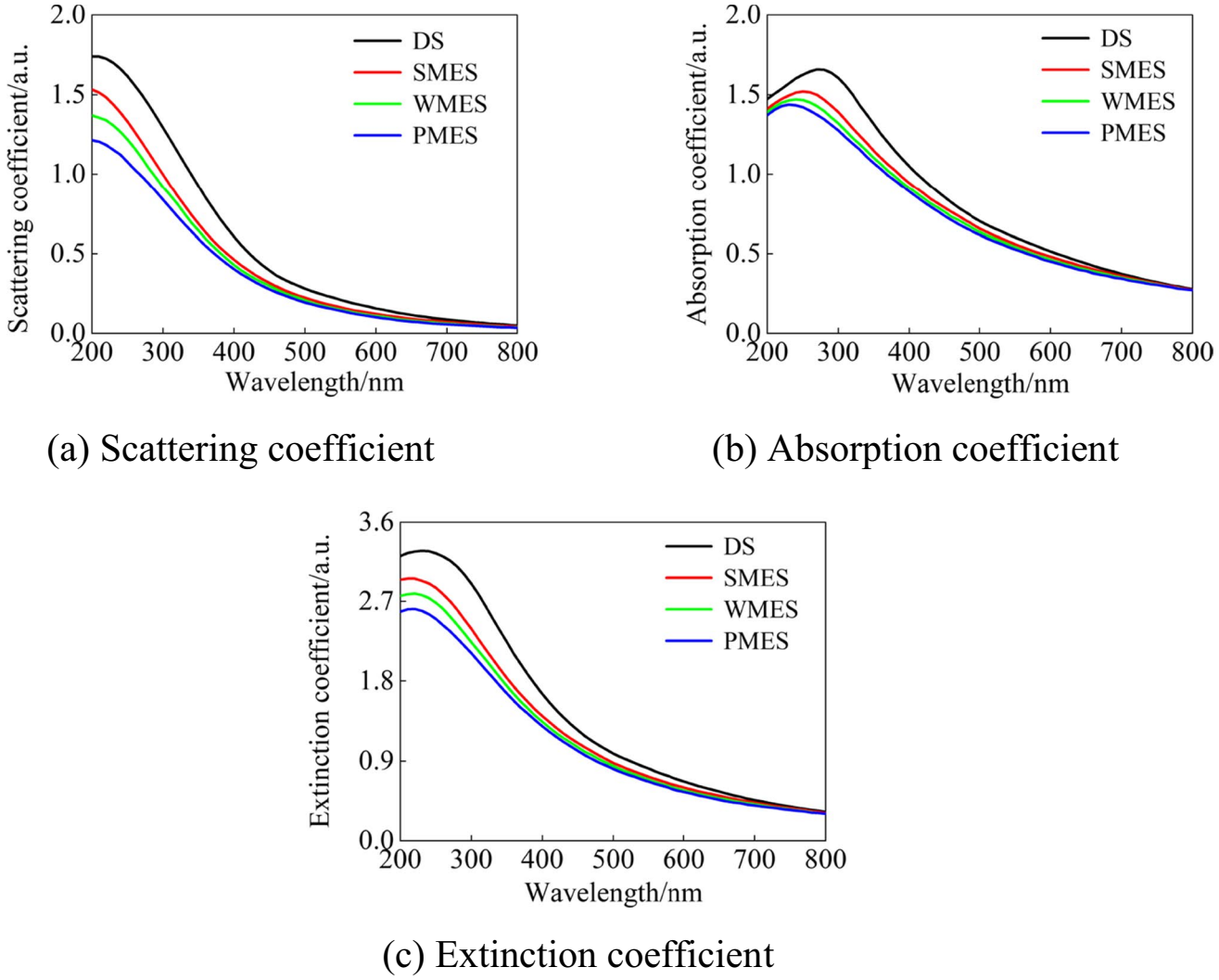

Fig. 15 The difference in extinction effect of PM from different fuels

than that of biodiesel, and the extinction ability of biodiesel decreases with iodine number decreasing, which means that the laser detection method of diesel can no longer accurately measure biodiesel PM emissions.

Conclusions

The particle size distribution, fractal dimension, and extinction characteristics of diesel and three kinds of SME, PME, and WME biodiesels were investigated on a 4-cylinder high-pressure common-rail diesel. The main conclusions are summarized as follows:

1. Biodiesel PM is smaller and more aggregated than diesel PM. Combustion biodiesel can reduce the number of particulate emissions by up to 84.2%. The average particle size of SMES, PMES, and WMES is 5.1%, 6.7%, and 13.9% lower than that of diesel particulate, respectively.
2. The extinction coefficient is highly sensitive to the particle size and fractal dimension of the PM. As the particle size increases, particle extinction coefficient gradually increases. The scattering coefficient of particles with a diameter of 100 nm is 17.27%, 11.46%, and 8.76% higher than that of particles with a diameter of 20 nm at three common kinds of light wave (wavelengths of 405 nm, 532 nm, and 781 nm, respectively). As the fractal dimension increases, the surface structure of the PM becomes more complex, and the effect of light absorption increases relatively, improving the dominant role of light absorption in extinction.
3. The number concentration and particle size of biodiesel PM is smaller than that of diesel PM. The decrease of

the iodine number of biodiesel will reduce the particle size, increase the fractal dimension, and lead to the weakening of the extinction characteristics.

Author contribution Siqi Ye: investigation, data curation, writing—original draft preparation. Dengpan Zhang: formal analysis, conceptualization, writing — reviewing and editing. Bo Chen: engine bench test. Jieping Xu: software, graph-visualization. Changkai Jia: data acquisition. Deqing Mei: methodology, writing — reviewing and editing. Yinnan Yuan: conceptualization, resources, funding acquisition.

Funding This work was supported by the National Natural Science Foundation of China (No. 51876133).

Data availability The datasets used and/or analyzed during the current study are available from the corresponding author on reasonable request.

Declarations

Ethical approval I would like to declare on behalf of my co-authors that the work described was original research that has not been published previously, and not under consideration for publication elsewhere.

Consent to participate Not applicable.

Consent for publication We confirm that the manuscript has been read and approved by all named authors and that there are no other persons who satisfied the criteria for authorship but are not listed. We further confirm that all the authors listed in the manuscript have been approved by all of us.

Competing interests The authors declare no competing interests.

References

Aizawa T, Nishigai H, Kondo K et al (2012) Transmission electron microscopy of soot particles directly sampled in diesel spray flame - a comparison between US#2 and biodiesel soot. SAE International Journal of Fuels and Lubricants 665-673. https://doi.org/10.4271/2012-01-0695

Alptekin E (2017) Emission, injection and combustion characteristics of biodiesel and oxygenated fuel blends in a common rail diesel engine[J]. Energy 119:44–52. https://doi.org/10.1016/j.energy.2016.12.069

Alptekin E, Canakci M, Sanli H (2012) Evaluation of leather industry wastes as a feedstock for biodiesel production[J]. Fuel 95:214–220. https://doi.org/10.1016/j.fuel.2011.08.055

Anis A et al (2021) Electrochemical stability analysis of red phosphorus-based anode for lithium-ion batteries. Electrochim Acta 395. https://doi.org/10.1016/j.electacta.2021.139149

Chai QM, Guo HY, Liu CY et al (2020) Global Climate Change and China's Action Plan – China's Climate Governance during the 14th Five-Year Plan (In writing). Yuejiang Academic Journal 12(06):36–58. https://doi.org/10.13878/j.cnki.yjxk.20210107.001

Chen WB et al (2022). Passive wireless temperature sensor based on equivalent localized surface plasmons. 41(06): 18–20+24. https://doi.org/10.13873/J.1000-9787(2022)06-0018-03

Cristina CM et al (2021) Can particulate matter be identified as the primary cause of the rapid spread of CoViD-19 in some areas of Northern Italy? Environ Sci Pollut Res 28(25):33120–33132. https://doi.org/10.1007/S11356-021-12735-X

Du JY, Yang QH, Zhang DP et al (2021) Effective of iodine value on the particle size distribution and carbon component of three biodiesel. J Xi'an Jiaotong Univ 55(05):18–24. https://doi.org/10.7652/xjtuxb202105003

Fredriksson H, Pakizeh T, Käll M et al (2009) Resonant optical absorption in graphite nanostructures. J Opt a: Pure Appl Opt 11(11):114022. https://doi.org/10.1088/1464-4258/11/11/114022

Gopinath A, Sairam K, Velraj R et al (2015) Effects of the properties and the structural configurations of fatty acid methyl esters on the properties of biodiesel fuel: a review. Proceedings of the Institution of Mechanical Engineers, Part d: Journal of Automobile Engineering 229(3):357–390. https://doi.org/10.1177/0954407014541103

He C, Li J, Wang Y et al (2017) Size-segregated particulate matter emission characteristics of a heavy duty diesel engine with oxygenated fuels. Appl Therm Eng 125:1173–1180. https://doi.org/10.1016/j.applthermaleng.2017.07.118

Huang JT, Wang DP (2021) Analysis of the physical origin of the red-shift of absorption peaks of conjugated polymers in solution. Chin J Appl Chem 38(11):1486–1493. https://doi.org/10.19894/j.issn.1000-0518.210138

Huang H, Zhou C et al (2016) An experimental study on the combustion and emission characteristics of a diesel engine under low temperature combustion of diesel/gasoline/n-butanol blends. Appl Energy 170:219–231. https://doi.org/10.1016/j.apenergy.2016.02.126

Huang H, Liu Q et al (2018) Improvement of combustion performance and emissions in diesel engines by fueling n-butanol/diesel/PODE3–4 mixtures. Appl Energy 227:38–48. https://doi.org/10.1016/j.apenergy.2017.09.088

Kuang Y, Guo Y, Chai J et al (2020) Comparison of light absorption and oxidative potential of biodiesel/diesel and chemicals/diesel blends soot particles. J Environ Sci 87:184–193. https://doi.org/10.1016/j.jes.2019.06.014

Laborde M, Crippa M, Tritscher T, et al (2013) Black carbon physical properties and mixing state in the European megacity paris. Atmos Chem Phys 13: 5831–5856. 1680–7316(2013)13:11<5831:BCPPAM>2.0.TX;2-#

László B et al (2022) Comparative study on the use of some low-cost optical particulate sensors for rapid assessment of local air quality changes [J]. Atmosphere 13(8):1218–1218. https://doi.org/10.3390/ATMOS13081218

Lawrence D, Krzysztof B, Geraint F (2021) Exploring the redshift-space peculiar velocity field and its power spectrum. J Cosmol Astropart Phys 2021(09). https://doi.org/10.1088/1475-7516/2021/09/018

Mei DQ, Wang Z, Yuan YN et al (2006) Analysis of the features of the particulate matters generated from diesel engine fueled with biodiesel. Transactions of the CSAE 22(12):113–116. https://doi.org/10.3321/j.issn:1002-6819.2006.12.024

Mei DQ et al (2019) Fractal morphology features and carbon component analysis of diesel particulates. Environ sci pollut res int 26(14):14014–14023. https://doi.org/10.1007/s11356-019-04783-1

Miyashita L et al (2021) Confocal microscopy 3D imaging of diesel particulate matter. Environ Sci Pollut Res 28(23):1–6. https://doi.org/10.1007/s11356-021-14025-y

Moore RH, Thornhill KL et al (2017) Biofuel blending reduces particle emissions from aircraft engines at cruise conditions. Nature 543(7645):411–5. https://doi.org/10.1038/nature21420

Moser BR (2014) Impact of fatty ester composition on low temperature properties of biodiesel-petroleum diesel blends[J]. Fuel 115(jan):500–506. https://doi.org/10.1016/j.fuel.2013.07.075

Nabi MN, Zare A et al (2017) Reductions in diesel emissions including PM and PN emissions with diesel-biodiesel blends. J Cleaner Prod 166:860–868. https://doi.org/10.1016/j.jclepro.2017.08.096

Nutakki PK et al (2021) Effect Of n-amyl alcohol/biodiesel blended nano additives on the performance, combustion and emission characteristics of CRDi diesel engine. Environ Sci Pollut Res 29(1):1–16. https://doi.org/10.21203/rs.3.rs-223789/v2

Qiu J, Liu LH, Hsu P (2010) FDTD analysis of infrared radiative properties of microscale structure aluminum surfaces[J]. J Quant Spectrosc Radiat Transfer 111(12):1912–1920. https://doi.org/10.1016/j.jqsrt.2010.04.026

Scheepers PT, Vermeulen RC (2012) Diesel engine exhaust classified as a human lung carcinogen. How will this affect occupational exposures? Occup Environ Med 69(10):691–3. https://doi.org/10.1136/oemed-2012-101088

Srinivasan SK, Kuppusamy R, Krishnan P (2021) Effect of nanoparticle-blended biodiesel mixtures on diesel engine performance, emission, and combustion characteristics. Environ Sci Pollut Res 28(29):1–17. https://doi.org/10.1007/s11356-021-13367-x

Stieb DM, Evans GJ, To TM et al (2020) An ecological analysis of long-term exposure to PM2.5 and incidence of COVID-19 in Canadian Health Regions. Environ Res 191:110052. https://doi.org/10.1016/j.envres.2020.110052

Takahashi K, Minoura H, Sakamoto K (2008) Examination of discrepancies between beta-attenuation and gravimetric methods for the monitoring of particulate matter[J]. Atmos Environ 42(21):5232–5240. https://doi.org/10.1016/j.atmosenv.2008.02.057

Tan PQ, Ruan SS et al (2014) Particle number emissions from a light-duty diesel engine with biodiesel fuels under transient-state operating conditions. Appl Energy 113:22–31. https://doi.org/10.1016/j.apenergy.2013.07.009

Wang T, Zhao G, Tan T et al (2021) Effects of biomass burning and photochemical oxidation on the black carbon mixing state and light absorption in summer season. Atmos Environ 248:118230. https://doi.org/10.1016/j.atmosenv.2021.118230

Wu G, Jiang GH, Yang ZY et al (2019) Particulate matter generation and emission characteristics of diesel engine fueled by biodiesel[J]. R Environ Sci 32(11):1809–1817. https://doi.org/10.13198/j.issn.1001-6929.2019.07.12

Xing J, Sun XG, Zhou S et al (2010) Complex refractive index measurement of fly ash particles using suspension spectral transmission method[J]. Spectroscopy and Spectral Analysis 30(12):3371–3374. https://doi.org/10.3964/j.issn.1000-0593(2010)12-3371-04

Zhang Y, Lou D et al (2018) Experimental study on the durability of biodiesel- powered engine equipped with a diesel oxidation catalyst and a selective catalytic reduction system. Energy 159:1024–1034. https://doi.org/10.1016/j.energy.2018.06.190

Zhang ZC et al (2021) Parameterization scheme for dry aerosols complex refractive index. China Environ Sci 41(2):580–587. https://doi.org/10.19674/j.cnki.issn1000-6923.2021.0066

Zhang CY, Lv QN, Zhang FG (2021) Particle size index measure based on the polarization distribution difference of scattered light[J]. Acta Optica Sinica 41(19):247–255. https://doi.org/10.3788/AOS202141.1929001